Bubble Trapping and Coalescence at the Baffles in Stirred Tank Reactors

Rahman Sudiyo
Dept. of Chemical Engineering, Gadjah Mada University, Jl. Grafika 2, Yogyakarta, Indonesia

Bengt Andersson
Dept. of Chemical and Biological Engineering, Chalmers University of Technology, S-41296 Gothenburg, Sweden

DOI 10.1002/aic.11250
Published online July 31, 2007 in Wiley InterScience (www.interscience.wiley.com).

Turbulent flow and bubble coalescence in water at the leeward side of a baffle in a stirred tank reactor have been studied with PIV and a high-speed CCD camera. A large stationary vortex was revealed at the leeward side of the baffle. At impeller speeds of 400–600 RPM, the maximum tangential velocity at the vortex was proportional to the impeller tip speed ($u_\theta \approx 0.27\ U_{tip}$), giving a pressure difference in the vortex of as much as a few hundred pascal. The main mechanism for coalescence in this area was trapping of bubbles in the vortex, increasing the local hold-up and coalescence probability by forcing the bubbles together. The force on the bubbles resulting from the local pressure gradient makes the bubbles move fast to the centre, within 10–20 ms. The coalescence efficiency was very high and more than 85% of the coalescence occurred within 2 ms. Bouncing of bubbles was mainly seen for large bubbles moving up in the centre of the vortex. The trapping of the bubbles was modeled successfully by a drag coefficient model corrected for nonspherical bubbles and turbulent continuous phase. © 2007 American Institute of Chemical Engineers *AIChE J,* 53: 2232–2239, 2007

Keywords: bubble coalescence, drainage time, stationary vortex, wake of baffles, turbulence, high speed camera, gas–liquid stirred tank reactor

Introduction

A balance of coalescence and breakage rate determines bubble size distribution, which is one of the most important factors controlling interfacial mass transfer rate in gas–liquid stirred tank reactors. The breakage occurs mainly in the impeller region, while coalescence occurs in the whole tank.[1] The importance of bubble coalescence in turbulent flow of such reactors has been suggested by several researchers.[2–6] The occurrence of bubble coalescence was indicated by the increase of Sauter mean diameter and the evolution of bubble size distribution. In most of the previous observations, however, bubble coalescence was lumped with the break-up, and thus a deep understanding of the coalescence process could not be obtained.

Studies of bubble coalescence have been performed by a number of researchers.[7–13] Unfortunately, these studies were done for a pair of bubbles under nonturbulent flow conditions. The results may not be applicable to bubble coalescence in turbulent flows.

Correspondence concerning this article should be addressed to B. Andersson at bengt.andersson@chalmers.se.

Bubble coalescence is generally considered as a three-step process, i.e., bubble collision, drainage of liquid film, and film rupture. In the case of low Weber number, i.e., in the absence of viscous forces, the film rupture occurs in less than 10 μs.[14] This is a very short period of time and truly negligible compared with the first two steps. The instantaneous process of film rupture has been confirmed by experimental findings of Ueyame et al.[11] As a consequence, once bubbles collide, film drainage is the only important issue. Models to predict drainage time related to bubble coalescence have been proposed by several researchers, such as Chesters and Hofmam,[14] Oolman and Blanch,[9] and Li.[12] Experimental data on drainage time are available for bubble coalescence in stagnant liquid,[9,11,13] whereas data on turbulent flow do not exist. The use of a high-speed CCD camera in the present work allows measurement of the film drainage, which is important in validating the existing models.

There are several mechanisms for bubble collisions in turbulent flows, as depicted in Figure 1. Turbulent transport by small or large turbulent eddies causing relative motion between bubbles is seen in Figures 1a,b. Figure 1c shows buoyancy-driven coalescence due to different rise velocities of different sizes of bubbles and to trapping in the bubble wake. Bubble collisions may also result from a velocity gradient, as seen in Figure 1d. Finally, bubbles trapped in large turbulent eddies or stationary vortices may collide. The relative importance of these mechanisms depends among other things on bubble size, size and energy of turbulent eddies, velocity gradient of the liquid phase, and the presence of stationary vortices.

In turbulent flows of a stirred tank, a stationary vortex is found on the leeward side of each baffle at the impeller plane.[15,16] Additionally, two trailing vortices originated from behind each blade can be seen as stationary vortices, since they are generated constantly at more or less the same position. The stationary vortices rotate fast, resulting in a low-pressure region within the vortices. Bubbles tend to be captured by the vortex core, leading to higher gas hold-up within the vortex, as shown experimentally by Sudiyo et al.[15] and Sudiyo[16] in the case of a stationary vortex on the leeward side of the baffle, and by Van't Riet and Smith[17] in the case of trailing vortices behind the impeller blade.

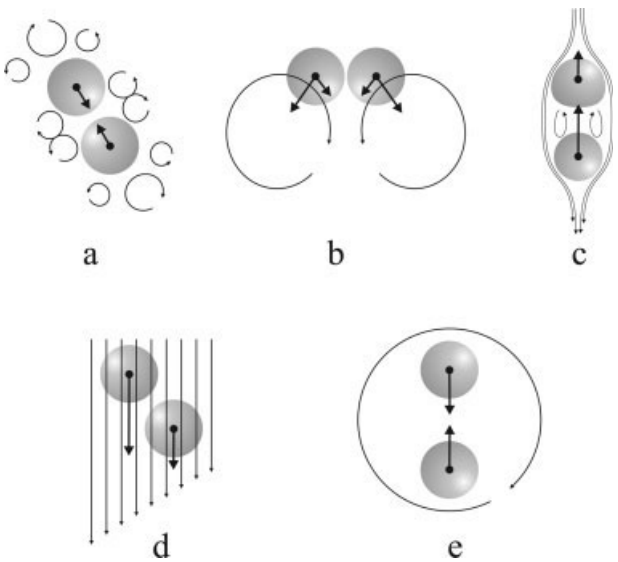

Figure 1. Different mechanisms of bubble collision.

The main objectives of the present work are to develop a model of bubble capture in a stationary vortex at the leeward side of the baffle, and to study the role of the vortex in enhancing bubble coalescence in this region. It is expected that the proposed concept of collision and coalescence processes following bubble capture can also be applied to other coalescence processes mentioned previously. As the position and orientation of the stationary vortex are relatively fixed, and located closer to the tank wall than trailing vortices or turbulent eddies, the choice of stationary vortex provides an easier way to develop a model for bubble capture, and to verify the model with experimental observations. The study has been performed in a pure air-water system, and we expect that the mechanism for trapping of bubbles is general and similar for ionic solutions and systems containing surfactants, but the coalescence mechanism will be very different.

Model Development

Vortex model

The stationary vortex found on the leeward side of the baffle will be considered as a Gaussian vortex.[18,19] This type of vortex has the following tangential velocity distribution:

$$u_\theta(r) = \frac{\Gamma_0}{2\pi r}\left(1 - e^{-\eta_1 (r/r_C)^2}\right) \tag{1}$$

where Γ_0, r_C, and η_1 are the fluid circulation, the core radius of the vortex, and a constant, respectively.

Equation 1 can be inserted into a radial momentum equation and then be integrated to yield[18]

$$p(r) - p_\infty = \int_\infty^r -\frac{\rho u_\theta^2(r)}{r} dr = \rho\left(\frac{\Gamma_0}{2\pi r_C}\right)^2 \left(\frac{1}{2(r/r_C)^2}\right) \left(\begin{array}{l} -1 + 2e^{-n_1 (r/r_C)^2} - e^{-2n_1 (r/r_C)^2} \\ -2\eta_1 (r/r_C)^2 Ei\left(\eta_1 (r/r_C)^2\right) \\ +2\eta_1 (r/r_C)^2 Ei\left(2\eta_1 (r/r_C)^2\right) \end{array}\right) \tag{2}$$

Equation 2 is obtained by assuming steady axisymmetric flow field with no gradient in radial velocity component and a constant density. The equation suggests that the pressure at the centre of the vortex is much less than that in the surrounding fluid, particularly for large values of $\frac{\Gamma_0}{r_C}$.

Capture of bubbles by the vortex

By assuming that the presence of gas bubbles does not significantly affect the flow, the equation of motion can be written as follows[19,20]:

$$\rho_B V_B \frac{dv_i}{dt} = V_B(\rho_B - \rho_f)g_i - V_B \frac{\partial p}{\partial x_i} + \frac{1}{2}\rho_f V_B \left(\frac{du_i}{dt} - \frac{dv_i}{dt}\right) + F_i^D + F_i^L + F_i^B + F_i^V \quad (3)$$

where ρ_B, ρ_f, and V_B are the gas density, the liquid density, and the bubble volume, respectively. The bubble velocity and the fluid velocity are denoted as $v_i(\mathbf{x},t)$ and $u_i(\mathbf{x},t)$. The terms on the right side of Eq. 3 represent the buoyancy force, the force because of pressure gradient of the undisturbed flow, the added mass force, the drag force F_D, the lift force F_L, the Basset history force F_B, and the force due to the change of bubble volume F_V.

In the present analysis, the buoyancy and the last three forces, F_L, F_B, and F_V, are neglected, as is also done by Oweis et al.[19] They showed that the use of different lift coefficients produces only little effect on the final solution of Eq. 3, suggesting that the lift force F_L does not play an important role. The force because of the change of bubble volume, F_V, is also neglected because the pressure reduction within the steady vortex is not large enough to result in a significant change of the bubble volume. The Basset history force, F_B, is neglected[19,21] as the acceleration of the relative motion of the bubble is generally small.

Equation 3 can be further simplified by assuming that the bubble initially rotates with the eddy, and that the largest component of bubble velocity is in the radial direction v_r. By doing so, Eq. 3 becomes

$$(\rho_B + \frac{1}{2}\rho_f)V_B \frac{dv_r}{dt} = \frac{u_\theta^2}{r}\rho_f V_B - C_D \frac{1}{2}\rho_f A_B v_r^2 \quad (4)$$

where u_θ is the tangential velocity of the fluid. The drag coefficient C_D is calculated with the following equations[22]:

$$\begin{cases} C_D = \frac{16}{Re_B} & Re_B < 1.5 \\ C_D = 14.9 Re_B^{-0.78} & 1.5 < Re_B < 80 \\ C_D = \frac{48}{Re_B}(1.0 - 2.21 Re_B^{-0.5}) & 80 < Re_B < 700 \end{cases} \quad (5)$$

Material and Methods

A cylindrical, flat-bottom mixing tank having four baffles (each 1.5 cm width) and a lid, with diameter of 15 cm, was used in the experiment. The tank, made of Plexiglass, is equipped with a six-blade Rushton disc turbine impeller with the diameter of one-third of the tank diameter. The impeller is placed at one-third of the tank diameter from the tank bottom. The tank was filled with water up to the height of 15 cm. Air was introduced into the tank by a needle located 2 cm below the impeller disc. To minimize optical distortion, the mixing tank was immersed in water. The experiments were performed at various stirrer speeds between 500 and 700 RPM at constant gas flow rate (276 cm^3/min).

The experiments were performed using two techniques: (1) video imaging, to observe bubble motions, bubble deformations, bubble size, and the coalescence rate; (2) particle image velocimetry (PIV), to measure local instantaneous velocity field of the liquid phase. The PIV measurements were conducted independently of the video imaging technique measurements without any bubble presence.

Measurements were carried out in different areas along the leeward side of one of the tank baffles. Both horizontal (r–θ) and vertical (r–z) plane measurements were carried out at different vertical distances, $H/6$, $H/3$, $H/2$, and $9H/10$, from the tank bottom (H is the liquid depth).

Depending on the orientation of the light source with respect to the camera and the optic, the video imaging technique can be differentiated into two: the shadowgraph (backlighted imaging) technique and the front light technique. The experimental set-up of the shadowgraph technique used in the present work is shown in Figure 2. To obtain high time resolution and high contrast, an Nd-Yag laser having a wavelength of 532 nm was used as the light source for generating an illumination plane. To get a homogeneous illumination plane, a light diffuser was used. The frequency of laser beam has been synchronized to the shutter speed of the CCD camera. For the horizontal (r–θ) plane measurements, a 150-W halogen lamp was used as the light source instead of the laser. The light from the halogen lamp was transmitted through a fibre-optic arm toward a light diffuser. The same

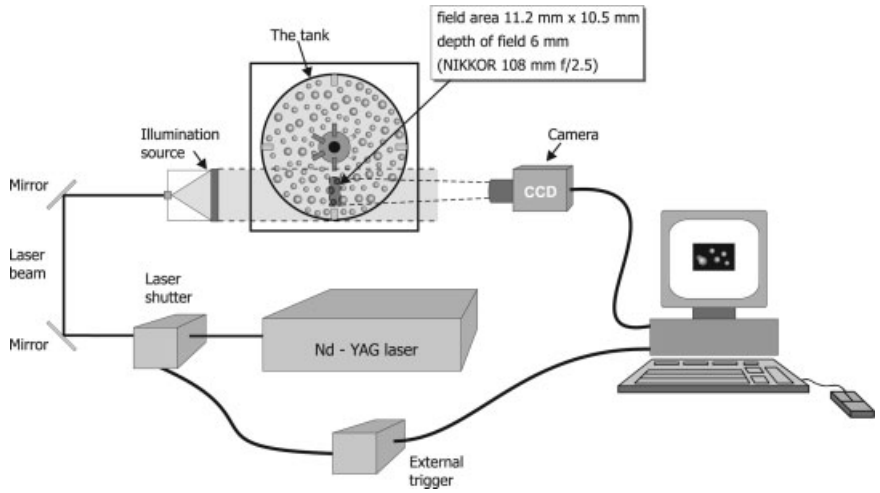

Figure 2. Experimental set-up of shadowgraph technique.

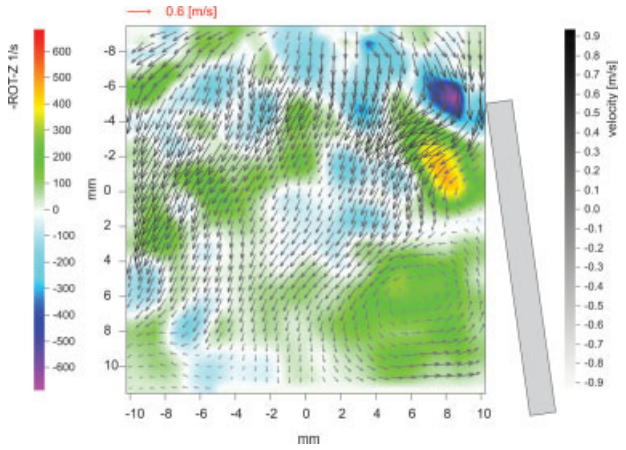

Figure 3. The measured instantaneous velocity field at the leeward side of the baffle at *H*/3 (the figure is perpendicular to the axis of the vortex).

[Color figure can be viewed in the online issue, which is available at www.interscience.wiley.com.]

lamp was used for the front light technique, but without the light diffuser. In r–θ plane measurements, a mirror was placed below the bottom of the tank to observe bubble motion captured by steady vortex.

The camera is a digital high-speed 10 bit CMOS having an array of 1280 × 1024 pixels at a frame speed of 625 s^{-1}, with the maximum frame speed of about 40,000 s^{-1} at a pixel resolution of 1280 × 16. All measurements were done at the frame speed of 1000 or 2000 s^{-1}frames/s with a pixel resolution of 1200 × 632 or 1200 × 321, respectively. Such high time and spatial resolution enable observation of the movement of bubbles and bubble coalescence.

The size of the measurement plane and its depth of field (DOF) are determined by the configuration of the receiving optics. A telephoto lens, Nikkor 105 mm, equipped with an extension separating the lens body from the CCD camera, is set at a big aperture. The configuration aims to produce quite large measurement volume, while keeping DOF small enough (about 5 mm) to enable the camera to produce sharp images. The size of measurement area obtained was 37 × 10 mm at the frame speed of 2000 s^{-1} and at the closest subject-camera distance. The minimum bubble size measured with reasonable accuracy was about 200 μm. All measurements were carried out for a period of 2 or 4 s for a frame speed of 2000 or 1000 s^{-1}, respectively, which is equivalent to 20 or 40 full rotations of the impeller at the speed of 600 RPM.

Instantaneous velocity fields obtained from PIV measurements[15] were then analyzed in terms of turbulent structures. A detailed description of the PIV measurements, including the experimental set-up and data handling, has been given by Sudiyo et al.[15] Turbulent structure is identified on the basis of Reynolds-decomposed fluctuations and vorticity analysis, as only the large-scale structures are of interest.[23] The small structures do not contain sufficient energy to significantly affect the bubble motions. The vorticity is expressed in Cartesian tensor notation as[24]

$$\varsigma_i = \varepsilon_{ijk} \frac{\partial u_k}{\partial x_j}. \tag{6}$$

where ε_{ijk} is the Levi–Cevita symbol.

Results and Discussion

Vortex characterization

On the basis of frame-to-frame analysis of the instantaneous velocity fields, the presence of vortex, i.e. any region of concentrated vorticity,[24] was observed. At all stirrer speeds investigated (400, 500, and 600 RPM), the measurements reveal the presence of a large stationary vortex at the leeward side of the baffle. An example of such a vortex is shown in the bottom right corner of Figure 3. The analysis also suggests that the vortex core is rather stationary. The amplitude of the movement of the vortex centre is less than 25% of the vortex core radius. It was indicated from measurements that the stationary vortex exists a few cm above and below the blade centreline (H/3) but its strength diminishes substantially at vertical distances of H/6 and H/2 from the reactor bottom.

Figure 4 (left) plots the measured and the predicted mean tangential velocities as functions of the radial distance from the vortex centre, at three different impeller speeds (400, 500, and 600 RPM). The calculated tangential velocity, applying the Gaussian vortex model Eq. 1, fits the measured tangential velocity quite well. As expected, higher stirrer speed produces a stronger vortex. However, if the tangential velocity shown in Figure 4 is normalized to the tip velocity of the impeller blade U_{tip}, all three curves representing dif-

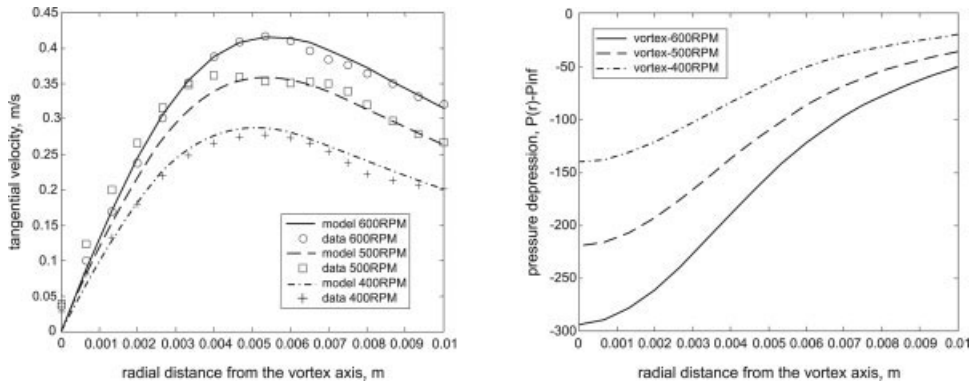

Figure 4. Radial distribution of tangential velocity (left image) and pressure (right image).

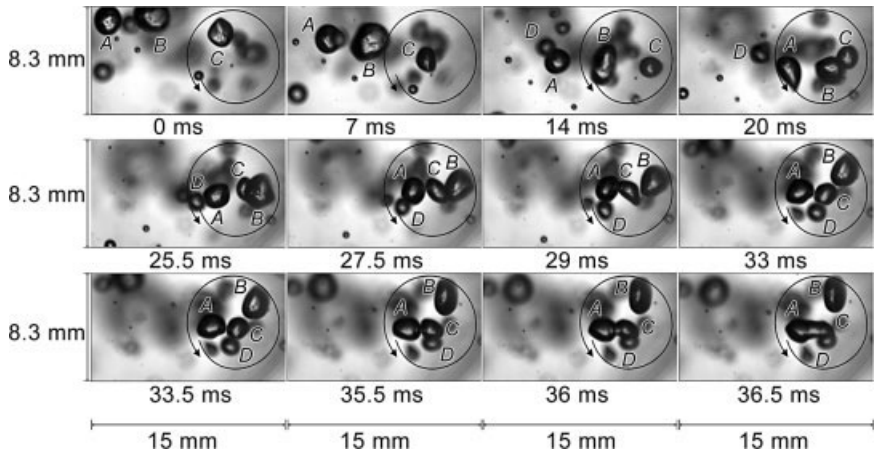

Figure 5. Bubbles captured by the stationary vortex followed by coalescence (r–θ plane).

ferent stirrer speeds converge into more or less a single curve with the maximum velocity of about 0.27 U_{tip}. The core radius (r_C), where the tangential velocity reaches its maximum value, occurs at a radial distance one-third of the baffle width from the vortex centre.

The radial pressure difference within the vortex can be estimated from Eq. 2 and the result is presented in Figure 4 (right). Depending on the stirrer speed, the pressure difference may vary from 120 to 240 N/m^2 giving a pressure gradient corresponding to 1.2–2.4 g. Even though the pressure difference is small compared with the absolute pressure of the system, such a pressure gradient is large enough to force bubbles in the vortex to move toward the vortex centre.

Bubble behavior

The pressure gradient draws gas bubbles in the vicinity of the impeller inwards toward the vortex core and leads to an increase of gas hold-up within the vortex, as shown in Figure 5. Both gas hold-up and the centrifugal force acting on bubbles increase the probability of bubble collisions. The centrifugal force because of the vortex rotation speeds up the drainage of the liquid that fills up the gap between the two bubbles approaching each another. The figure, which was taken by shadowgraph technique from the bottom of the tank (r–θ plane), also shows collision and coalescence of the captured bubbles inside the vortex.

In analyzing the stationary vortex-captured bubbles, two origins of bubbles are being considered: first those coming from the lower part of the tank, and second those from the impeller discharge stream and from the windward (front) side of the baffle. In the first case, bubbles pass the vortex on rising up to the liquid surface. Figures 6 and 7 show typical examples of vortex-captured bubbles for the first and second cases, respectively. These figures were taken vertically, in the r–z plane, at the frame speed of 1000 s^{-1}. In the opposite direction of the impeller rotation, the vortex rotates anticlockwise around an axis which is more or less parallel to the axis of the impeller shaft.

The two bubbles being captured by the vortex shown in Figure 6, which finally collide and coalesce, come from the left edge of the frame, i.e., from the *impeller discharge stream*. The change of the bubble's appearance from clear to blurred indicates the motion of bubbles out of the plane of the paper (away from the reader) toward the vortex centre. A similar situation can be seen in Figure 7 where the two bubbles coming from the lower part of the tank are captured by the vortex.

The movement of bubbles into the stationary vortex is caused not only by the convective flow from the impeller or by buoyancy from below, but also by turbulent dispersion. Figure 8 shows the Reynolds-decomposed fluctuation and the average velocity fields at the leeward side of the baffle and its surroundings, measured in the r–θ plane. As seen in Figure 8 (left), the area at the leeward side of the baffle is quite turbulent, with the average turbulent intensity about 9%. The random motions of the large turbulent eddies carry bubbles into the vicinity of the stationary vortex.

Bubble capture time

One of the important factors that influence the rate of coalescence is the ratio of capture time (time required for bubble to move to the vortex center) and residence time of the bubble in the vortex region. In this work, capture time was based on the bubble movement from 0.8 to 0.25 of the core radius. As defined previously, the core radius is a radial distance from the vortex centre where the tangential velocity reaches its maximum value (Figure 4). Figure 9 shows the capture

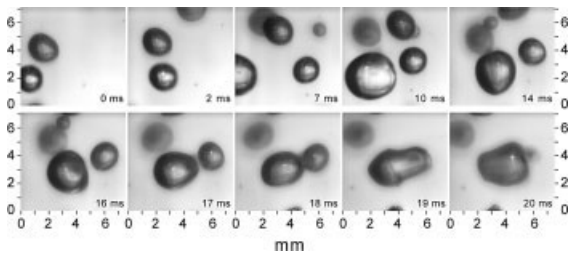

Figure 6. Coalescence of two vortex-captured bubbles (for second case).

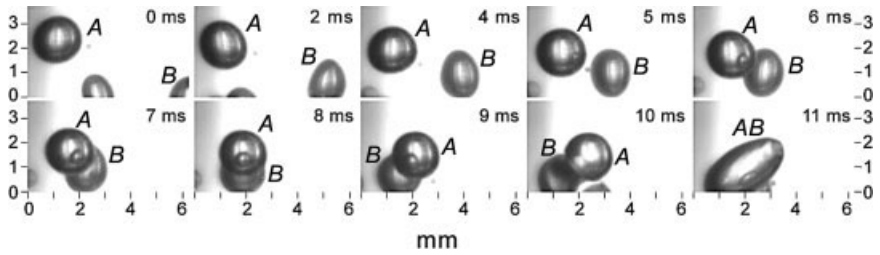

Figure 7. Coalescence of two vortex-captured bubbles (for first case).

time of bubbles of different size at impeller rotational speed of 500 RPM.

Data shown were taken from measurement in the horizontal (r–θ) plane, from which more accurate estimation on the capture time can be obtained. The turbulence in the continuous phase is assumed to be the cause of scattered data. As expected, large bubbles require less time to move toward the vortex centre than do small ones. While the driving force (the pressure gradient induced by the centrifugal force) increases with r_B^3, the dominant retarding force (the drag force) increases with r_B^2 or r_B at low Re. As seen in Figure 9, the acceleration of the virtual mass becomes the dominant retarding force for large bubbles and the capture time becomes independent of bubble size. A correction factor for the drag coefficient needs to be introduced, as the drag coefficient shown in Eq. 5 is for the laminar flow in the continuous phase, while in fact the flow in the current work is highly turbulent. In comparison with the measured capture time, the capture time calculated from Eq. 4 shows a quite encouraging agreement.

Equation 4 is derived by assuming that the presence of gas bubbles does not significantly alter the liquid flow. To validate this assumption, the angular velocity of the liquid phase obtained by using the PIV technique in the absence of gas bubbles was compared with that obtained from measuring the angular velocity of bubbles as illustrated in Figure 10. While the two bubbles are forced to move toward the vortex centre, they also rotate with an average angular velocity of about 80 rad/s. Such high angular velocity is not far from the angular velocity of the instantaneous liquid velocity shown in Figure 3. Frame-to-frame observation of more than 30 similar situations (Figure 10) shows that the average angular velocity is about 100 rad/s, which is more or less similar to the angular velocity of the average liquid velocity shown in Figure 8 (the right image).

Bubble coalescence

Figure 10 shows a coalescence of two large bubbles on the leeward side of the baffle at the impeller plane, at the frame speed of 2000 s^{-1}. Flattening of the bubble surfaces against each other prior to film drainage is shown in the figure. The flattening occurs twice, i.e. following the elapsed times of 20.5 and 29 ms (see second row in Figure 10), but the first flattening does not lead to coalescence. However, such clear bubble surface flattening occurs very rarely.

The drainage time, further referred to as coalescence time, is defined as the time required from the onset of film drainage until film rupture. It is common to assume the onset of bubble flattening as the onset of the drainage. However, a sharp onset of bubble flattening does not exist in reality and therefore cannot be used as the starting point in determining coalescence time experimentally. As done by Ueyama et al.,[11] the present work considers the moment of the first contact of two bubbles leading to coalescence as the starting point in determining coalescence time, instead of the onset of bubble flattening.

On the basis of the above definition, the coalescence time of bubbles shown from 28 ms elapsed time in Figure 10 is very short (usually less than 2 ms). The moment of bubble collision at elapsed time 20.5 ms is not considered as the

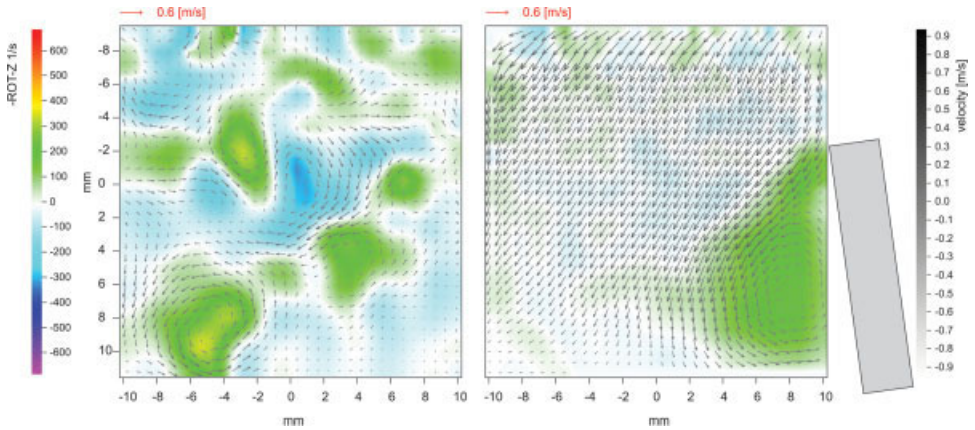

Figure 8. Velocity and vorticity fields measured at the leeward side of the baffle, the left and the right image show the fluctuating and the average velocity fields (the vortex axis is perpendicular to the plane of the figure).

[Color figure can be viewed in the online issue, which is available at www.interscience.wiley.com.]

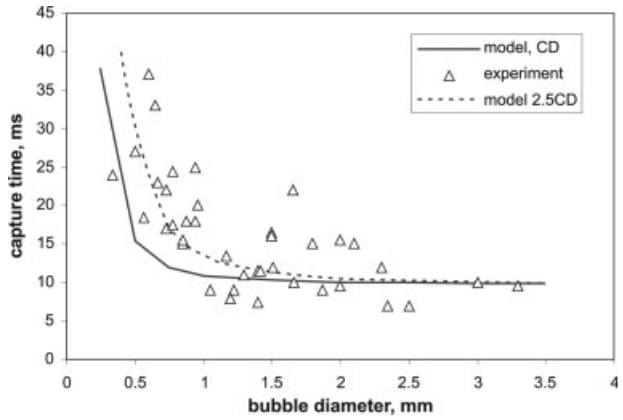

Figure 9. Measured and predicted capture time as function of bubble diameter.

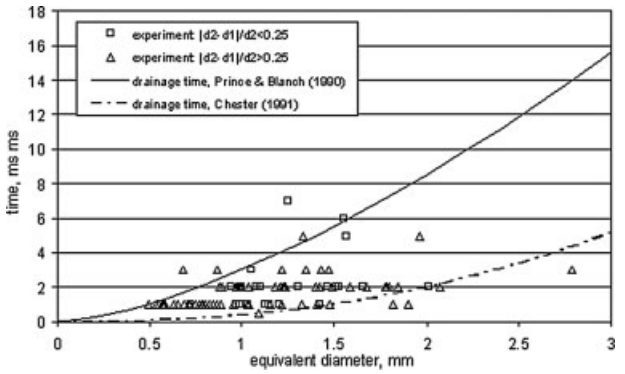

Figure 11. Comparison between the measured drainage (coalescence) time with those predicted by empirical correlation.

starting point, since it does not lead to bubble coalescence. All other coalescence events shown in Figures 5–7 also suggest very short coalescence times. Figure 11 shows a relation between coalescence time and equivalent bubble diameter, defined as $d_{eq} = 2 \cdot d_1 \cdot d_2/(d_1 + d_2)$. Total 93 coalescence events were observed, and 86% of them occurred within 2 ms or less, suggesting that the bubbles coalesced almost instantaneously. The coalescence time in turbulent flow using pure system in the present study is shorter than what was obtained in stagnant liquid in similar system.[9,11,25]

The effect of bubble size on the drainage time has never been reported in the previous experimental works. However, Ueyama et al.[11] used a laser technique to study the effect of a decrease in the approach velocity of the two bubbles being collided on the drainage time, and showed that the time remains constant as the velocity decreases from 4.17 to 0.42 mm/s. Considering that the trapped liquid film disk develops according to the approach velocity, they suggest that the drainage time does not depend on the growth rate of the disk radius. Further, they argued that the bubble size has a minor effect on the drainage time since as the growth rate of the film disk directly depends on the curvature of the bubble surface. This seems to be in agreement with data presented in Figure 11.

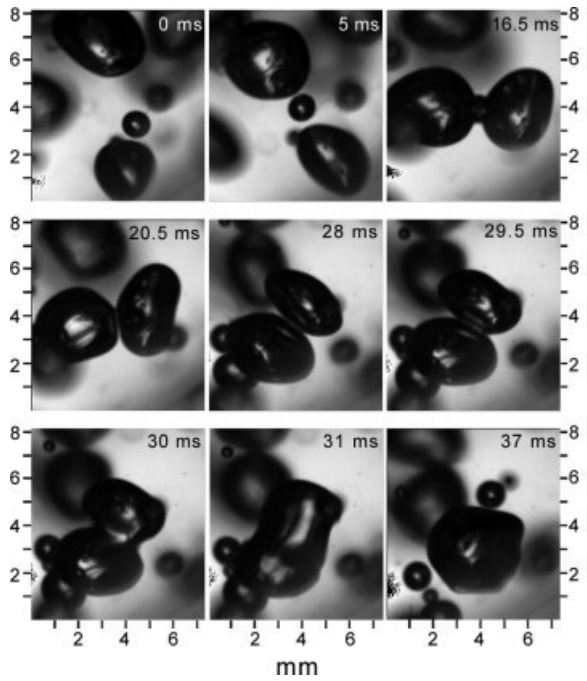

Figure 10. Two large bubbles coalesce as they rotate inside the vortex (the vortex axis is perpendicular to the plane of the figure).

It can be seen in Figure 11 that the parallel film theory of Prince and Blanch[26] overestimates the drainage time. The initial diameter of the liquid film disk in this theory is assumed to be the same as that of the bubble radius. This leads to a higher amount of water to drain and a longer drainage time. While both equations proposed by Prince and Blanch[26] and Chesters[8] are based on the parallel film theory, the equation proposed by Chester[8] allows the thickness, pressure, and radial velocity to vary along the radial direction of the film disk, leading to the development of "dimples", i.e. rings of minimum film thickness, during the drainage process. Here the film rupture occurs locally at the dimple ring and forms a hole. The formed hole then expands very rapidly and the bubbles become a unity unite. As shown in Figure 11, this results in a very short predicted coalescence time since only a small amount of water needs to be drained.

Conclusion

The high coalescence rate observed on the leeward side of tank baffles is mainly due to the increased hold-up and the additional force on the bubbles resulting from the local pressure gradient of the rotating stationary vortex. Because of the vortex rotation, the liquid filling the gap between two bubbles that approach each other in the center of the vortex moves out. At the impeller speeds used in the present work, the force acting on a bubble in the rotating vortex is on the order of 1.2–2.4 g. It is also more effective than buoyancy, since it is directed towards the centre of the vortex forcing the bubbles together, while buoyancy is directed in the same direction and it is only the difference between the forces that push the bubbles together.

Acknowledgments

Financial support from the programs Selective Preparation of Fine Chemicals and Pharmaceuticals, SELCHEM via the Swedish Foundation for Strategic Research, SSF, and SIDA in Swedish Research Links Programme are gratefully acknowledged. The assistance from Linda Hellström with various parts of the layout of the figures is also appreciated.

Literature Cited

1. Sudiyo R, Andersson B, Irandoust S, Bouaifi M. Bubble size and coalescence rate in gas-liquid stirred tank reactor: experimental and theoretical investigation. In: *17th International Symposium on Chemical Reaction Engineering*, Hong Kong, 2002.
2. Bakker A. *Hydrodynamics of stirred gas-liquid dispersions*. PhD Thesis. Delft University of Technology, Delft, 1992.
3. Barigou M, Greaves M. Bubble-size distributions in a mechanically agitated gas-liquid contractor. *Chem Eng Sci*. 1992;47:2009–2025.
4. Takahashi K, Nienow AW. Bubble sizes and coalescence rates in an aerated vessel agitated by a rushton turbine. *J Chem Eng Jpn*. 1993;26:536–542.
5. Alves SS, Maia CI, Vasconcelos JMT. Experimental and modelling study of gas dispersion in a double turbine stirred tank. *Chem Eng Sci*. 2002;57:487–496.
6. Laakkonen M, Alopaeus V, Aittamaa J. Validation of bubble breakage, coalescence and mass transfer models for gas-liquid dispersion in agitated vessel. *Chem Eng Sci*. 2006;61:218–228.
7. Marrucci G. A theory of coalescence. *Chem Eng Sci*. 1969;24:975–985.
8. Chesters AK. The modeling of coalescence processes in fluid-fluid dispersions: a review of current understanding. *Trans IChemE Part A: Chem Eng Res Des*. 1991;69A:259–270.
9. Oolman TO, Blanch HW. Bubble coalescence in stagnant liquids. *Chem Eng Commun*. 1986;43:237–261.
10. Kim JW, Lee WK. Coalescence behavior of two bubbles in stagnant liquids. *J Chem Eng Jpn*. 1987;20 5:448–453.
11. Ueyama K, Saeki M, Matsukata M. Development of system for measuring bubble coalescence time by using a laser. *J Chem Eng Jpn*. 1993;26:308–314.
12. Li D. Coalescence between small bubbles: effect of surface tension gradient and surface viscosities. *J Colloid Interf Sci*. 1996;181:34–44.
13. Thoroddsen ST, Etoh TG, Takehara K, Ootsuka N. On the coalescence speed of bubbles. *Phys Fluids*. 2005;17:071703.
14. Chesters AK, Hofman G. Bubble coalescence in pure liquids. *Appl Sci Res*. 1982;38:353–361.
15. Sudiyo R, Virdung T, Andersson B. Important factors in bubble coalescence modeling in stirred tank reactors. *Can J Chem Eng*. 2003;81:557–565.
16. Sudiyo R. *Hydrodynamics of gas-liquid flows and bubble coalescences in gas-liquid stirred tanks*. Thesis of Licentiate of Engineering. Departement of Chemical Engineering and Environmental Science, Gothenburg, Chalmers, 2003.
17. Van't Rieat K, Smith JM. The behaviour of gas-liquid mixture near Rushton turbine blade. *Chem Eng Sci*. 1973;28:1031–1037.
18. Oweis GF, Choi J, Ceccio SL. Dynamics and noise emission of laser induced cavitation bubbles in a vortical flow field. *J Acoust Soc Am*. 2004;115:1049–1058.
19. Oweis GF, van der Hout IE, Iyer C, Tryggvason G, Ceccio SL. Capture and inception of bubbles near line vortices. *Phys Fluids*. 2005;17:022105.
20. Maxey MR, Riley JJ. Equation of motion for a small rigid sphere in a nonuniform flow. *Phys Fluids*. 1983;26:883–889.
21. Oey RS, Mudde RF, van den Akker HEA. Sensitivity study on interfacial closure laws in two-fluid bubbly flow simulations. *AIChE J*. 2003;49:1621–1636.
22. Lain S, Bröder D, Sommerfeld M. Experimental and numerical studies of the hydrodynamics in a bubble column. *Chem Eng Sci*. 1999;54:4913–4920.
23. Piirto M, Eloranta H, Ihalainen H, Saarenrinne P. 2D spectral and turbulence length scale estimation with PIV. *J Vis*. 2001;4:39–44.
24. Green SI. Introduction to vorticity. In: Green SI, editor. *Fluid Vortices*. Netherlands: Kluwer Academic, 1995:1–9.
25. Tse K, Martin T, McFarlane CM, Nienow AW. Visualization of Bubble coalescence in a coalescence cell, a stirred tank and a bubble column. *Chem Eng Sci*. 1998;53:4031–4036.
26. Prince MJ, Blanche HW. Bubble coalescence and break-up in air-sparged bubble columns *AIChE J*. 1990;36:1485–1499.

Manuscript received Jan. 10, 2007, and revision received May 18, 2007.